

Nucleation of helium in liquid lithium

J.Martí, F.Mazzanti, G.E.Astrakharchik, L.Batet^{*}

*Department of Physics, Polytechnical University of Catalonia-Barcelona Tech,
B5-209 Northern Campus, Jordi Girona 1-3,
08034 Barcelona, Catalonia, Spain.*

L.Portos-Amill, B.Pedreño

*Barcelona School of Telecommunications Engineering,
Polytechnical University of Catalonia-Barcelona Tech, B3 Northern Campus,
Jordi Girona 1-3, 08034 Barcelona, Catalonia, Spain.*

(Dated: July 21, 2021)

Abstract

Fusion energy stands out as a promising alternative for a future decarbonised energy system. To be sustainable, future fusion nuclear reactors will have to produce their own tritium. In the so-called breeding blanket of a reactor, the neutron bombardment of lithium will produce the desired tritium, but also helium, which can trigger nucleation mechanisms owing to the very low solubility of helium in liquid metals. An understanding of the underlying microscopic processes is important for improving the efficiency, sustainability and reliability of the fusion energy conversion process. A spontaneous creation of helium drops or bubbles in the liquid metal used as breeding material in some designs may be a serious issue for the performance of the breeding blankets. This phenomenon has yet to be fully studied and understood. This work aims to provide some insight on the behavior of lithium and helium mixtures at experimentally corresponding operating conditions (843 K and pressures between 0.1 and 7 GPa). We report a microscopic study of the thermodynamic, structural and dynamical properties of lithium-helium mixtures, as a first step to the simulation of the environment in a nuclear fusion power plant. We introduce a microscopic model devised to describe the formation of helium drops in the thermodynamic range considered. A transition from a miscible homogeneous mixture to a phase-separated one, in which helium drops are nucleated, is observed as the pressure is increased above 0.175 GPa. The diffusion coefficient of lithium ($2 \text{ \AA}^2/\text{ps}$) is in excellent agreement with reference experimental data, whereas the diffusion coefficient of helium is in the range of $1 \text{ \AA}^2/\text{ps}$ and tends to decrease as pressure increases. The radii of helium drops have been found to be between 1 and 2 \AA .

I. INTRODUCTION

Within the framework of future energy supply, with the constraints posed by the need of electrification of the final energy demand, and the quest for more sustainable power generation methods in order to achieve a decarbonised electricity system, nuclear fusion energy stands out as a promising alternative. The fusion reaction that results most convenient in the present state of technological development is:

$$\text{D} + \text{T} \rightarrow {}^4\text{He} + \text{n} + 17.6 \text{ MeV}, \quad (1)$$

* jordi.marti@upc.edu, ferran.mazzanti@upc.edu, grigori.astrakharchik@upc.edu, lluis.batet@upc.edu

where 'D' stands for deuterium, 'T' for tritium and 'n' for a free neutron and where helium is a by-product[1]. Deuterium is abundant in water, but tritium ($t_{1/2}=12.3$ year) must be artificially created. Therefore, in order for fusion energy to be sustainable, it is necessary that tritium be produced in the reactor itself. Tritium will be generated by means of the reactions of neutrons escaping from the plasma with lithium in the so-called breeding blankets (see for instance [2] for an overview of these relevant components in DEMO, a demonstration power plant contemplated in the European Roadmap to Fusion). Breeding blankets (BB) will perform two additional functions besides producing tritium: extraction of fusion heat, and shielding the magnets (superconducting coils) from the radiation escaping the plasma.

Lithium has two natural isotopes ^6Li (abundance 7.5 %) and ^7Li (92.5 %), both producing tritium when capturing a neutron[3]:



Tritium self-sufficiency will require a certain neutron multiplication in order to close the fuel cycle with a net gain so that the so-called tritium breeding ratio is greater than 1. In order to fulfill their functions, some BB designs feature solid (ceramic) breeders cooled by helium, while others rely on a liquid metal (LM) cooled by helium or water. Usually the components of BB designs are lithium-lead eutectic (LLE)[2, 4, 5]. Besides ^7Li , lead will provide some fast neutron multiplication (neutrons hit the walls of the reaction chamber with energies bigger than 14 MeV). As shown in Eqs.(2) and (3), He is produced mol-to-mol along with T. However, He is practically insoluble in the liquid metal (Henry's constant for helium in Li at 843 K would be around $7 \times 10^{-14} \text{ Pa}^{-1}$ atomic fraction; for LLE it is estimated to be lower[6]). Tritium self-sufficiency requirement is thus linked to a possible super-saturation of helium in the liquid metal and, consequently, to a possible nucleation of helium in the form of bubbles. This phenomenon may have a great impact in the performance of the BB: changes in the magnetohydrodynamic flow, affectation of the heat transfer, and changes in the tritium migration mechanisms. Other systems that could be affected by helium nucleation are, for instance, free-surface Li first wall concepts[7, 8] and the Li jet targets in the future International Fusion Materials Irradiation Facility[9].

In the quest for tools to model the effect of the undesired helium bubbles being formed

in the blanket walls of a nuclear fusion plant, helium nucleation models must be developed. So far, no experiment exists allowing to validate such models. The low solubility of He in LM makes computer simulations extremely expensive if trying to capture the onset of nucleation at the design operational pressures and temperatures of BB. To provide an order of magnitude, a rough estimation based in the Gibbs' Classical Nucleation Theory [10, 11] (CNT) follows from Ref. [12]. At a temperature of 843 K some 40 atoms of He are needed to form a stable cluster when He concentration is 6 times larger than its solubility (see Fig. 1). A simulation involving 40 atoms of lithium at 843 K and 1 bar would require almost 10^9 atoms of lithium to be in those conditions. If Henry's law is valid at high pressures, only 1000 atoms of lithium would be necessary at 100 GPa.

This work focuses on the simulation of He-Li mixtures at high pressures as a first step towards the simulation of the Li-Pb-He mixtures at low pressure. The goal is to capture the onset of the nucleation in order to advance towards the modeling of the phenomenon. In this work we describe a mixture of helium and lithium atoms in the bulk, developing a microscopic model that is able to reproduce the helium-lithium mixture instability towards nucleation of helium drops, and performing ab-initio simulations of occurring processes. The Li-Li, He-He and He-Li pair interactions are fed as an input to both classical Monte Carlo (MC) and molecular dynamics (MD) simulations. We find thermodynamic, structural and dynamic properties of lithium and helium mixtures at high temperatures and in a wide range of pressures. Both MC and MD computational techniques have been previously proven to provide reliable predictions for a wide variety of classical and quantum atomic and molecular systems, ranging from pure quantum systems including hydrogen and helium[13–18] to classical molecular liquids in solution[19–23] and at interfaces[24–26] and to highly complex biosystems such as proteins or membranes[27–30]. We calculate and report thermodynamic properties such as the average internal energy as a function of pressure. In order to quantify the spatial and dynamical structure we calculate the pair distribution functions, the mean squared displacements, and the velocity autocorrelation functions. We also obtain the diffusion coefficient of lithium and helium at different pressures ranging from 0.1 to 10 GPa as well as the spectral densities of He and Li, reporting information on their main vibrational modes.

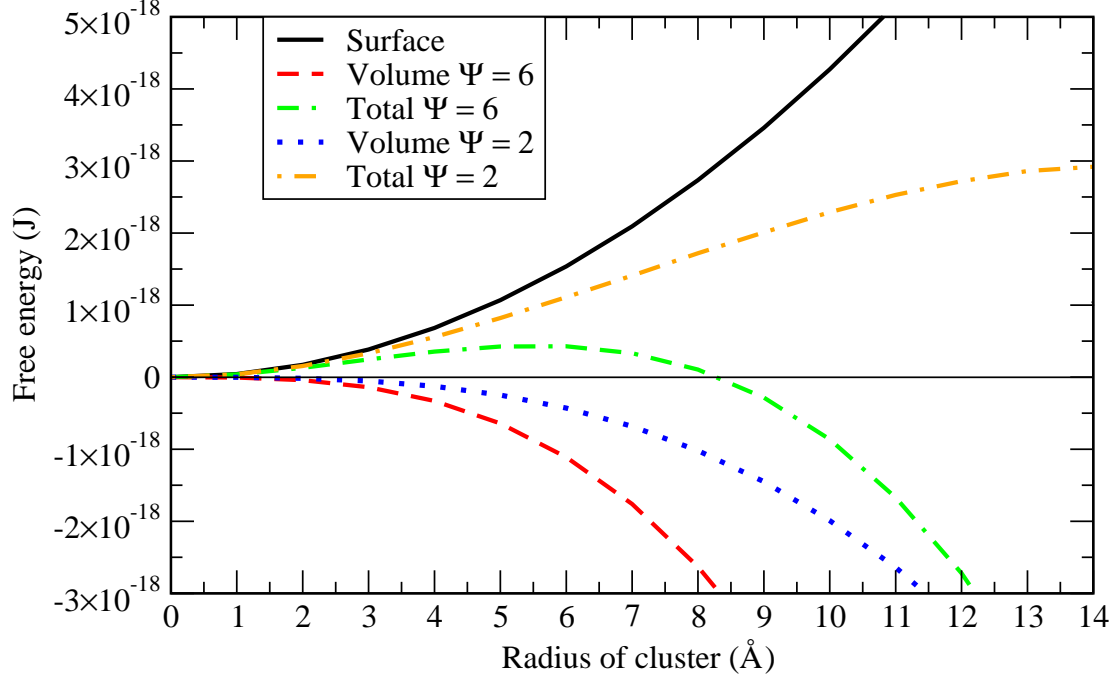


FIG. 1. Free energy of a cluster of He forming in lithium at 843 K assuming a surface tension of 0.34 N/m [31]. Using a volume of 17 \AA^3 for helium[12] critical size is 42 atoms when supersaturation ratio $\Psi = 6$ and 110 atoms when $\Psi = 2$.

II. METHODS

A. Microscopic model

We base our simulations on a microscopic model Hamiltonian describing a mixture of N_{Li} lithium and N_{He} helium atoms, which are taken to be point-like particles of mass m_{Li}

and m_{He} , respectively. In order to reproduce the experimental conditions, we only consider situations where $N_{\text{Li}} \gg N_{\text{He}}$. Each species is characterized by particle coordinates and velocities $\{\mathbf{r}_{\text{Li},i}, \mathbf{v}_{\text{Li},i}\}$ and $\{\mathbf{r}_{\text{He},j}, \mathbf{v}_{\text{He},j}\}$, with i and j spanning the ranges $1, \dots, N_{\text{Li}}$ and $1, \dots, N_{\text{He}}$, respectively. The Hamiltonian of the system is then written as

$$H = \frac{1}{2} \sum_{i=1}^{N_{\text{Li}}} m_{\text{Li}} v_{\text{Li},i}^2 + \frac{1}{2} \sum_{i=1}^{N_{\text{He}}} m_{\text{He}} v_{\text{He},i}^2 \quad (4)$$

$$+ \sum_{i < j}^{N_{\text{Li}}} V_{\text{Li-Li}}(|\mathbf{r}_{\text{Li},i} - \mathbf{r}_{\text{Li},j}|) + \sum_{i < j}^{N_{\text{He}}} V_{\text{He-He}}(|\mathbf{r}_{\text{He},i} - \mathbf{r}_{\text{He},j}|) + \sum_{i=1}^{N_{\text{Li}}} \sum_{j=1}^{N_{\text{He}}} V_{\text{Li-He}}(|\mathbf{r}_{\text{Li},i} - \mathbf{r}_{\text{He},j}|),$$

where the first two terms describe the kinetic energy, while the last three terms account for the intra- and inter-species interaction, respectively. Periodic boundary conditions are applied in order to minimize the finite-size effects and approximate better the properties of a large system. The typical simulation cage is a square box of length around 29 Å for the reference pressure of 1 GPa. In lower pressure setups, box lengths are larger than 40 Å.

A crucial point of our model is an appropriate choice of the pair interaction potentials. For lithium-lithium interactions (5) we rely on the model proposed by Canales et al. in Ref. [32, 33], whereas the remaining interactions are a novelty of the present work. The Li-Li pair interaction potential is modeled as [32, 33]

$$V_{\text{Li-Li}}(r) = Ar^{-12} + B \exp\{Cr\} \cdot \cos D(r - E), \quad (5)$$

where r is the distance between the two atoms in Angströms, $V(r)$ is measured in Kelvin units and the potential coefficients are $A = 2.22125 \times 10^7 \text{ K Å}^{12}$, $B = 41828.9 \text{ K}$, $C = -1.20145 \text{ Å}^{-1}$, $D = 1.84959 \text{ Å}^{-1}$, $E = 5.03762 \text{ Å}$. The interaction potentials are shown in Fig. 2 and they feature strong short-distance repulsion caused by Pauli exclusion due to overlapping electron orbitals, and a highly non-monotonic behavior which eventually follows a van-der-Waals attractive tail at large distances. The characteristic length of the interaction potential corresponds to the smallest distance at which the interaction changes sign, $V_{\text{Li-Li}}(\sigma_{\text{Li-Li}}) = 0$, and is equal to $\sigma_{\text{Li-Li}} = 2.5668 \text{ Å}$. The characteristic energy scale is defined by the depth of the first minimum, equal to $\epsilon_{\text{Li-Li}} \equiv V_{\text{Li-Li}}(3.06) = -887.9 \text{ K}$.

The helium-helium interaction has been considered to be of the Lennard-Jones (LJ) type, and it has been parameterized to accurately describe the system at the temperatures and

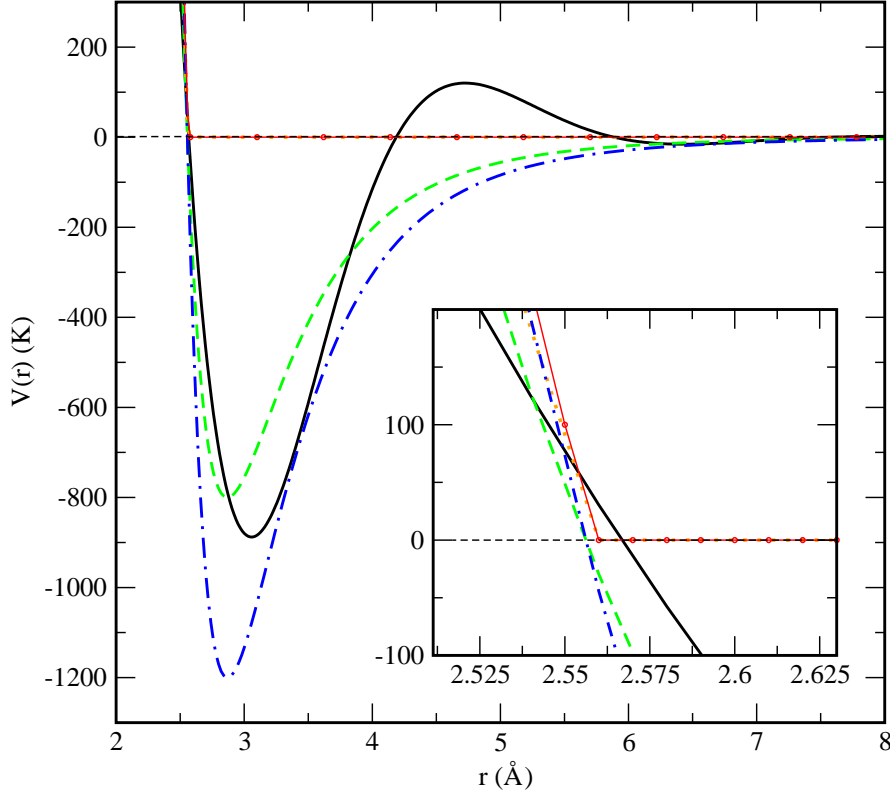


FIG. 2. Microscopic two-body interaction potentials employed in this work. Main figure: overall view of the interaction potentials $V(r)$ for Li-He, He-He and Li-Li as given by Eqs. (5-7). Li-Li (black line); He-He model 1 (dot-dashed blue line); He-He model 2 (dashed green line); Li-He model 1 (red circles) and Li-He model 2 (dotted orange lines). The inset represents a zoom of the “hard-wall” area at short distances.

pressures of interest which are well beyond ambient conditions. From preliminary simulations, we have found that the Aziz II interaction potential[34], which is known to provide an excellent description of superfluid liquid helium at temperatures close to absolute zero and moderate pressures around saturation density, does not work appropriately at the temperatures as high as 843 K and pressures in the GPa regime considered in the present study. Instead, we retain the same width $\sigma_{\text{He-He}} = 2.556 \text{ \AA}$ but treating the potential depth $\epsilon_{\text{He-He}}$ as a free adjustable parameter. In this work we have found that, in order to be able to

reproduce the nucleation process, the depth must be increased to the typical values of the Li-Li potential (5). In order to test the influence of this interaction parameter, we considered two different values of the potential depth, $\epsilon_{\text{He-He}} = -1200$ K and $\epsilon_{\text{He-He}} = -800$ K, referred to as “model 1” and “model 2”, respectively.

Finally the helium-lithium interactions have been modeled through a Lennard-Jones potential at short distances, namely a “hard” wall, with characteristic parameters given by the Lorentz-Berthelot rules obtained from the corresponding Li-Li and He-He values, and a cutoff beyond that point. This results in $\sigma_{\text{Li-He}} = 2.5615$ Å and $\epsilon_{\text{Li-He}} = -1032.2$ K. The potential model is given by:

$$V_{\text{Li-He}}(r) = 4\epsilon_{\text{Li-He}} \left[\left(\frac{\sigma}{r} \right)^{12} - \left(\frac{\sigma}{r} \right)^6 \right], \quad r \leq \sigma_{\text{Li-He}} \quad (6)$$

$$= 0, \quad r > \sigma_{\text{Li-He}}$$

The four considered pairwise interactions are shown in Fig. 2. In a very recent work [35], it has been reported that specific interatomic potentials based on Daw-Baskes and Finnis-Sinclair formalisms are able to describe the formation of helium bubbles in a palladium tritide lattice at temperatures of the order of 400 K and pressures in the range of 0.1 to 2.2 GPa. Furthermore, the formation of helium bubbles in tungsten was also reproduced using purely repulsive He-W interaction potentials in cluster simulations[36], models rather close to the ones presented in this work.

B. Monte Carlo and molecular dynamics methods

We rely on MC and MD methods to perform a series of computer simulations of the system. Both methods use the microscopic model as reported in Eq. (4) to describe interactions between the atoms as an input and allow for the calculation of the thermodynamic quantities of interest.

The Monte Carlo method has been used to obtain the equilibrium properties at fixed pressure P , particle number N and temperature T . This is done starting from the microscopic Hamiltonian of Eq. (4) and sampling from it the corresponding Maxwell-Boltzmann distribution, where the probability of a state with energy E is $p = \exp(-E/k_B T)$, using the standard Metropolis algorithm. Once the system has thermalized, we perform simulations

to estimate properties such as the energy per particle and volume, as well as correlation functions such as the pair distribution function and the low-momentum static structure factor. An advantage of the MC method is that it only uses the particle positions, in contrast to MD where their velocities have also to be sampled. This halves the number of microscopic variables to estimate, thus reducing the phase space and making the exploration very efficient. This, however, comes at a price, since Monte Carlo can only sample equilibrium configurations, and therefore it is not able to provide information about the time-dependent properties, in contrast to MD where the simulation propagates in real time.

In molecular dynamics, the force fields are also obtained from the model in Eq. (4) and the corresponding Newton's equations of motion, which are integrated numerically using a standard leap-frog Verlet procedure[37]. In every simulation, we have considered a fixed number of particles N and pressure, P while the volume is adjusted correspondingly. In addition to the energetics and structural properties obtained also in MC, MD provides access to time-dependent quantities such as the diffusion coefficient, velocity autocorrelation functions and spectral densities. As a stringent test of self-consistency, strict agreement between the common quantities sampled in MC and MD has to be obtained, which requires the proper thermalization and averaging in both methods.

III. RESULTS

A. Thermodynamic states

In all cases a homogeneous mixture of helium and lithium has been considered as the starting point of the simulations. The concentration of helium has been set to ~ 0.04 for a total of 40 helium atoms dissolved in a sea of 960 lithium atoms. The main results for the thermodynamic quantities of interest obtained in both MC and MD are summarized in Table I. Additional simulations at intermediate pressures (0.3 and 0.4 GPa for instance) have also been considered in several other sections of the manuscript.

As a starting point of our analysis, we have obtained average internal energies and pressures of all considered simulation runs, as reported in Table I. In the MC simulations, the system was initially allowed to equilibrate for a total of 10^7 MC random movements and spanning a total time of about 50 ps for the MD simulations. After that and in order to

collect statistics the system was allowed to evolve for another 10^8 random steps during the MC simulations. Correspondingly, we collected MD trajectories 200 ps long in all cases. In both MC and MD statistical errors were less than 1% in all reported quantities. The state of lowest internal energy is found at the pressure of 1 GPa. As an additional test, in order to explore the influence of helium concentration on the total energy of the system, we report energies as a function of the relative helium concentrations in Figure 3. We defined the relative helium concentration p as

$$p = \frac{n_{\text{Li}} - n_{\text{He}}}{n_{\text{Li}} + n_{\text{He}}} \quad (7)$$

We observe a monotonic behaviour at the lowest pressure (0.1 GPa), that becomes non-monotonic for the second pressure (0.3 GPa). This might be an indication of a different qualitative phase coexistence for the two selected pressures. We report further information about this aspect in the following sections.

B. Pair distribution functions

In order to quantify the spatial correlations and visualize the structure of helium drops, we calculated the pair distribution function (RDF) in the simulated mixture of 960 Li and 40 He atoms at 843 K. The RDF is defined as

$$g_{\alpha,\beta}(r) = \frac{1}{N_{\alpha}N_{\beta}} \sum_{i=1}^{N_{\alpha}} \sum_{j=1}^{N_{\beta}} \langle \delta(|\mathbf{r}_{ij} - r|) \rangle \quad (8)$$

where α, β identify the species and the $\langle \dots \rangle$ denotes a thermal average. Being a two-particle correlator, it can measure translationally invariant ordering, suitable to identify drop formation independently of its center of mass position. Typical RDF for Li-Li, Li-He and He-He pairs are shown in Fig. 4 for different pressures. The shape of the Li-Li pair distribution functions is characteristic of a liquid at equilibrium. Li-Li RDF are hardly affected by the presence of a small concentration of helium atoms, as can be seen in comparison with the behaviour of pure lithium at 1 GPa and the same temperature, taken from Ref. [33]. One might also note that a change by a factor of 100 in the pressure does not significantly change the overall shape of $g_{\text{Li-Li}}(r)$. The short-range region is voided due to the steep potential cores. Strong oscillations are visible at separations comparable to

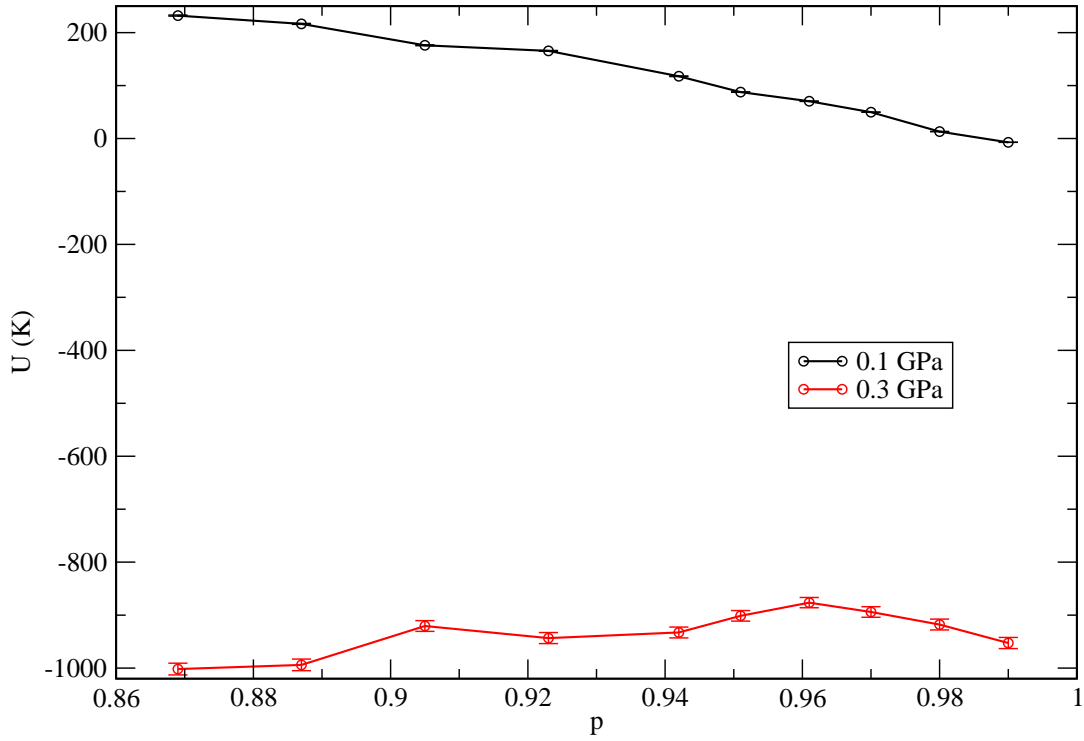


FIG. 3. Total internal energies U as a function of concentration p for two characteristic pressures (0.1-0.3 GPa).

the mean interparticle distance, witnessing strong correlations in the liquid, inducing shell effects. At large distances, the pair distribution function approaches a constant value, thus confirming that lithium atoms are homogeneously filling the whole space. The situation is drastically different in the He-He RDF, as they vanish at large distances as seen in Fig. 4(c). While at low pressure, $g_{\text{He-He}}$ still shows a long-range plateau, this is not the case for large pressure where the RDF strongly decreases. This implies that helium atoms concentrate close to each other, thus forming droplets. In this way, helium atoms form a miscible mixture on a lithium background at low pressure, but have a tendency to phase separate at large pressures, splitting the system into pure lithium and helium phases. This scenario is further supported by the huge increase in the height of the first and subsequent shells in a

He drop. The drop size can be roughly estimated as the difference between the distance at which $g_{\text{He-He}}(r)$ significantly decays (position of the first minimum) and the position of the starting non-zero value of the RDF.

In order to verify the robustness of our analysis, we have compared the results obtained with the two different He-He potential models proposed corresponding to a depth well of 800 K and 1200 K, to find only minor changes. We have observed that when this depth is above 650 K, helium drops are not well formed and become significantly unstable in short time intervals of the order of 1 ps. From here on, the reported results are those corresponding to model 1, as it predicts more stable helium droplets.

A set of four characteristic snapshots of the system at pressures $P = 0.1, 0.2, 1$ and 10 GPa is shown in Fig. 5 to illustrate the tendency of the system to form helium droplets when P is increased above approximately 0.2 GPa. At lower pressures helium is fully diluted in the lithium bath. This is also seen in the He-He pair distribution function, which is shown in Fig. 6 for several values of P close to the critical transition pressure. There we can observe that helium drops start to appear at a crossover pressure around 0.175 GPa, which corresponds to phase separation (helium droplets in liquid lithium), while full stable ones showing up at 0.2 GPa.

In order to further characterize the phase separation, we are also reporting static structure factors $S(k)$ computed from the RDF (Eq. 9) for low momenta ($k = 0.216 \text{ \AA}^{-1}$) as a function of the pressure:

$$S(k) = 1 + 4\pi\rho_0 \int_0^\infty dr r(g_{\alpha,\beta}(r) - 1) \sin kr, \quad (9)$$

where $g_{\alpha,\beta}(r)$ is given by Eq. 9, and ρ_0 is the average density of each species (α, β). The results are shown in Fig. 7. The change in the slope of $S(k)$ is particularly sharp in the He-He case, around the crossover pressure of 0.175 GPa, differently of the cases of Li-Li and Li-He. It has recently reported for the Ising model [38] that the sensibility of changes in slope of static structure factors may be a clear indication of a possible phase transition. The precise quantification of such a phase transition is currently evaluated in our lab, although it is out of the scope of the present work.

The radii of helium droplets formed in our simulations are reported in Table II and represented in Fig. 8 while the specific size depends on the amount of particles in the simulation. We considered only the reference case of 40 Helium and 960 lithium atoms. One

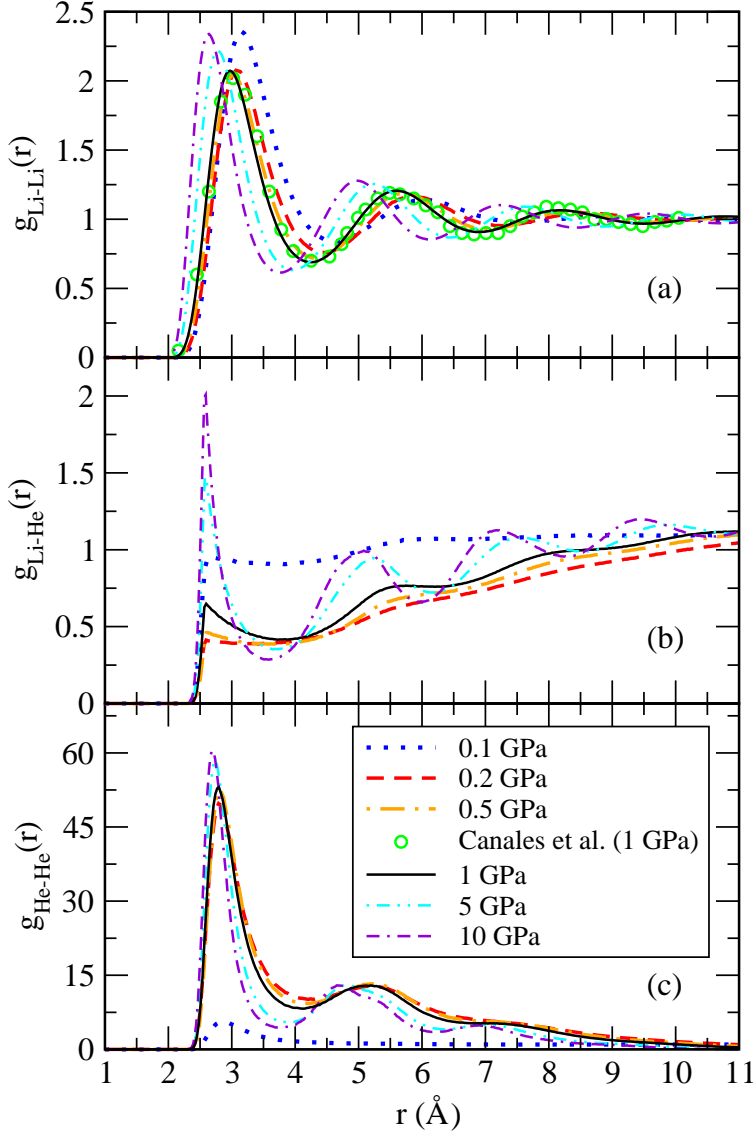


FIG. 4. Pair distribution functions in a wide range of pressures (0.1-10 GPa) quantifying (a) He-He (b) He-Li (c) Li-Li correlations. Green circles, single-species Li-Li data from Ref. [33]. Lines: 0.1 GPa (dotted blue); 0.2 GPa (dashed red); 0.5 GPa (dot-dashed orange); 5 GPa (dot-dot-dashed cyan); 10 GPa (dash-dash-dotted violet).

observes that the radius is largest at low pressures thus decreasing as the pressure increases. At pressures below 1 GPa, we can fit an exponential law: $R = 1.965e^{-0.12P}$ (P in GPa) whereas in the range above 1 GPa, the best fit is linear: $R = 1.84 - 0.05P$. This indicates a qualitatively different behaviour for R , strongly dependent on the pressure.

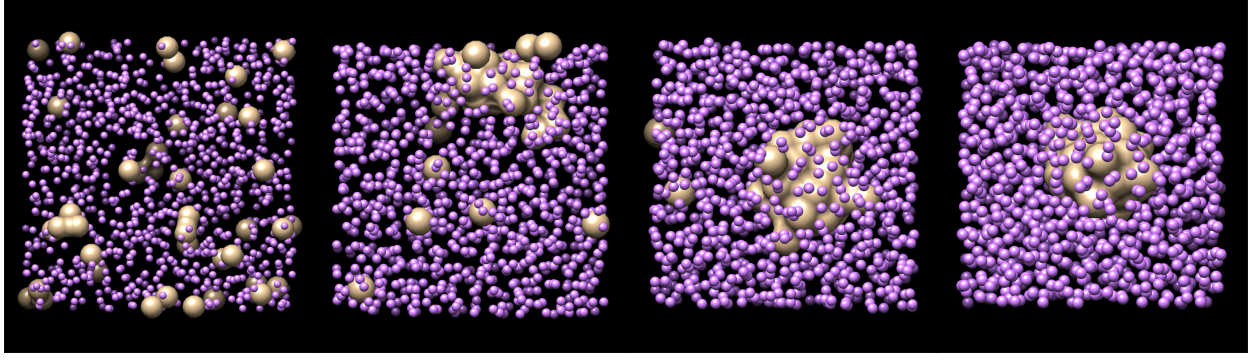


FIG. 5. Snapshots of the He-Li mixtures at characteristic pressures: 0.1 GPa, 0.2 GPa, 1 GPa, 10 GPa (increasing pressure from left to right).

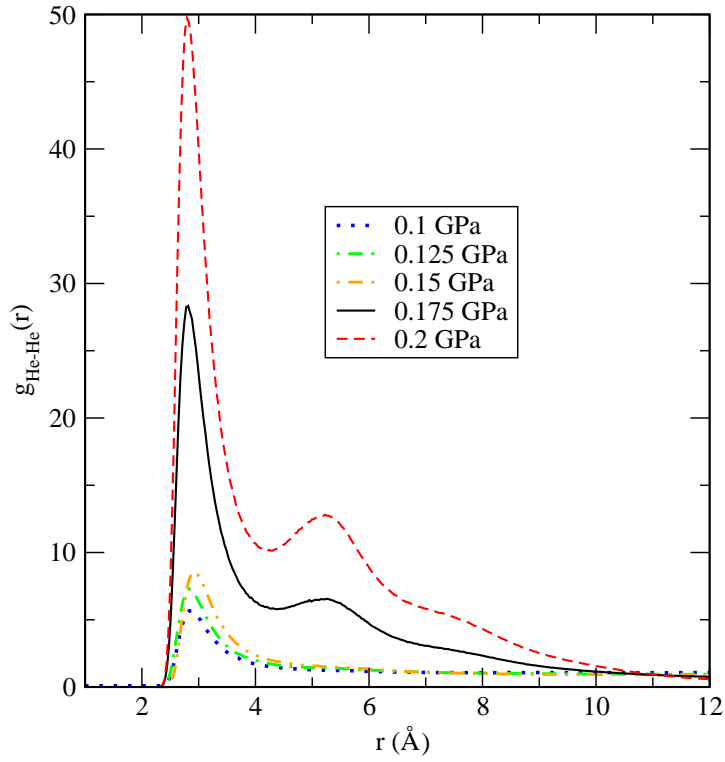


FIG. 6. He-He pair distribution functions in the vicinity of the phase-separation transition (0.1-0.2 GPa). Lines: 0.1 GPa (dotted blue); 0.125 GPa (dot-dashed green); 0.15 GPa (dot-dot-dashed orange); 0.175 GPa (black); 0.2 GPa (dashed red).

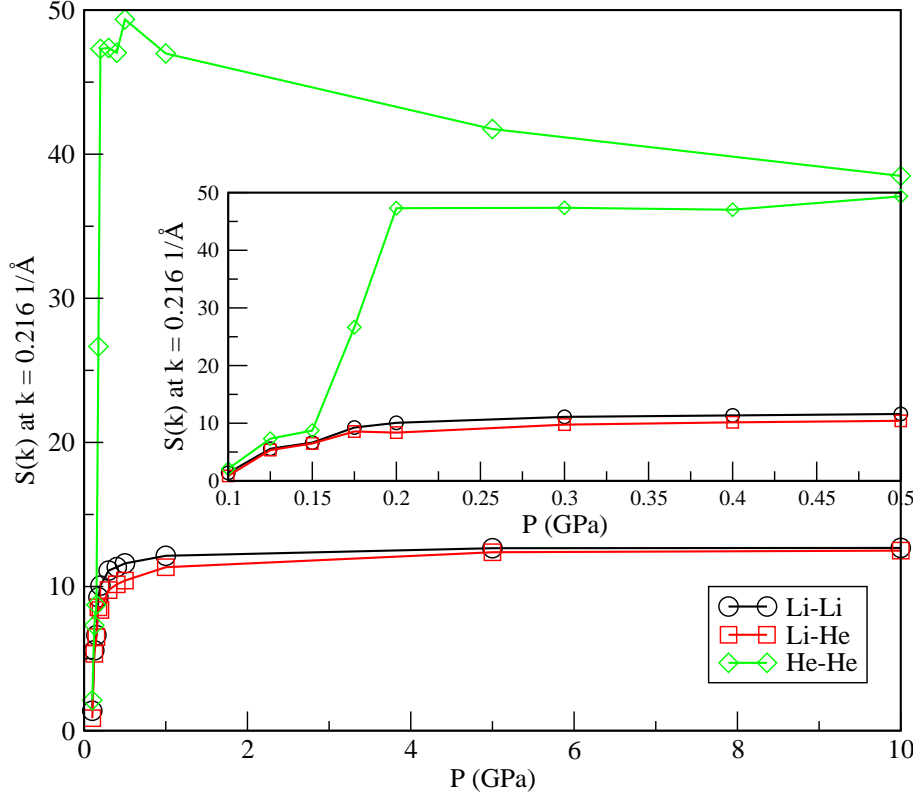


FIG. 7. Static structure factors computed at very low momentum ($k = 0.2161/\text{\AA}$) a function of the pressure. Li-Li (black circles); Li-He (red squares); He-He (green diamonds).

C. Atomic diffusion

Another experimentally relevant quantity is the diffusion coefficient. Using the molecular dynamics method, the mean square displacement (MSD) for both helium and lithium was separately obtained. The value of the diffusion coefficient D was then computed from the slope of the steady-state MSD, using Einstein's formula

$$D = \frac{1}{6} \lim_{t \rightarrow \infty} \frac{d}{dt} \langle |\mathbf{r}(t) - \mathbf{r}(0)|^2 \rangle, \quad (10)$$

where \mathbf{r} stands for the coordinate of each species (lithium, helium). The coefficients at all simulated states are reported in Table III. Canales et al. [33] obtained a value for

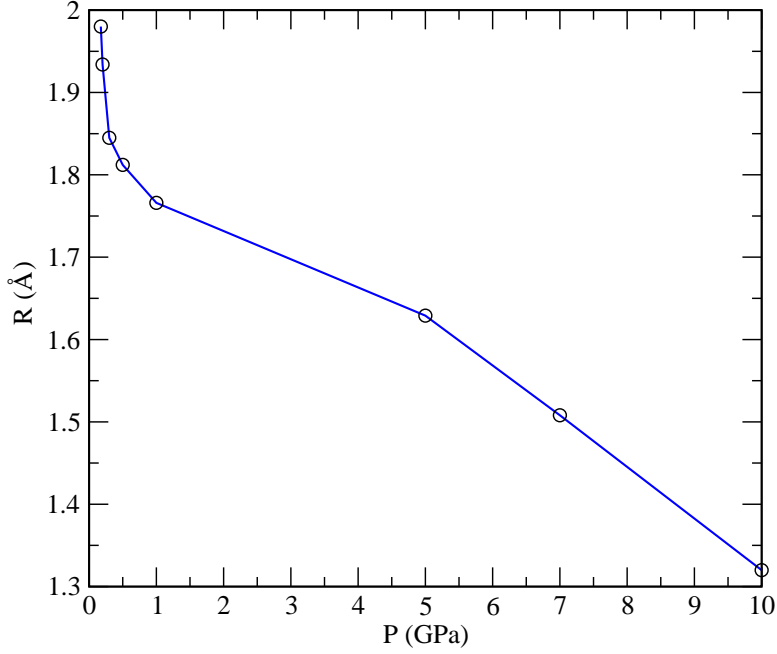


FIG. 8. Radii of helium droplets for the pressure range 0.175-10 GPa.

the diffusion coefficient of pure lithium at 843 K (around 1 GPa) of $2.47 \text{ Å}^2/\text{ps}$, whereas Jayaram et al. [39] reported $0.8 \text{ Å}^2/\text{ps}$ at 500 K. Our result at 843 K is of $D = 2.0 \text{ Å}^2/\text{ps}$, indicates that the lithium diffusion coefficient does not change significantly from its value in the absence of helium. This is not surprising considering the low concentration of helium atoms examined. It is also worth noticing that the experimental value of $45 \text{ Å}^2/\text{ps}$ at 523 K, reported by Nieto et al. [40] for helium injected onto the surface of a stream of flowing lithium corresponds to a system out of equilibrium, which is a different situation from the one analyzed here. This can explain the large difference of two orders of magnitude when compared to our result, $0.833 \text{ Å}^2/\text{ps}$ at 843 K and 1 GPa (see Table III). Experiments in other similar systems might provide a more suitable reference to compare our results to. Figure 9 shows the values of D obtained in our simulations as a function of the pressure. As

it can be seen, the dependence of D on P is approximately linear, showing slower diffusion at pressures above 1 GPa.

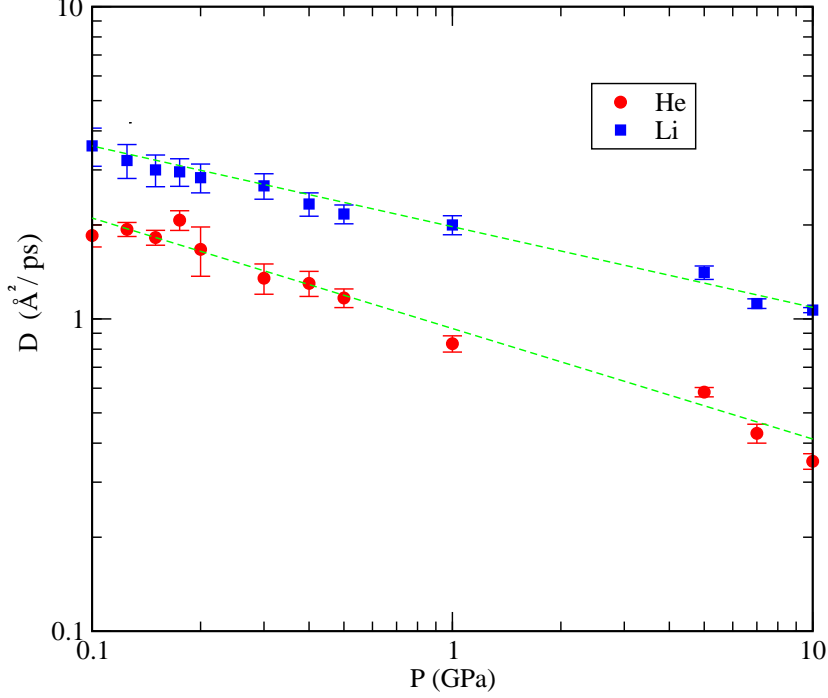


FIG. 9. Diffusion coefficients of lithium (blue squares) and helium (red circles) at 843 K as a function of the of the pressure on a double-logarithmic scale. Green straight lines are a guide to the eye.

D. Atomic spectroscopy

Experimental infrared spectra are usually obtained through the absorption coefficient $\alpha(\omega)$ or the imaginary part of the frequency-dependent dielectric constant[41]. These properties are directly related to the absorption lineshape $I(\omega)$, which can also be obtained from molecular dynamics simulations[42–44] in certain situations. In most cases the physically

relevant property to be computed is the so-called atomic spectral density $S_i(\omega)$, defined as:

$$S_i(\omega) = \int_0^\infty dt \langle \vec{v}_i(t) \vec{v}_i(0) \rangle \cos(\omega t) \quad (11)$$

where $\vec{v}_i(t)$ is the velocity of the i -th atom at time t , while the brackets $\langle \dots \rangle$ denote an equilibrium ensemble averaging. In our case we have obtained the spectral density of each atomic species separately. Generally speaking, classical molecular dynamics simulations are not able to fully reproduce experimental absorption coefficients, these being quantum properties. However they can be used to locate the position of the spectral bands since in the harmonic (oscillator) approximation, classical and quantum ground state frequencies are equal.

The power spectrum describes the main vibrational modes of a molecular system, including low frequencies below 100 ps^{-1} , associated with translational and rotational modes, and high frequencies of stretching and bending vibrations around and above 500 ps^{-1} . The power spectra were obtained for the velocity autocorrelation functions (VACF) of lithium and helium atoms and are shown in Fig. 10. We find that lithium atoms have a tendency to oscillate at frequencies between 30 and 85 ps^{-1} , whereas the vibrational frequency for helium atoms is between 2 and 100 ps^{-1} , approximately. The fact that these peaks are found at low frequencies is consistent with a picture where the atoms in our system can only present translational vibration modes [45].

IV. CONCLUDING REMARKS

In this work we have analysed the structure and dynamics of lithium-helium mixtures with a very low He concentration as a first step towards the simulation of the typical environmental conditions in the BB of a fusion power plant. We perform ab-initio simulation of the lithium-helium mixture using Monte Carlo and molecular dynamics methods, which yield the same predictions at equilibrium. Monte Carlo method is more efficient for the calculation of thermodynamic quantities and we employ it for the estimation of the total energy and pressure, along with some of its structural properties as the pair distribution functions. From molecular dynamics we have obtained, in addition, time-dependent quantities such as the diffusion coefficients, velocity autocorrelation functions for the atoms in the mixture, as well as power spectra of the latter.

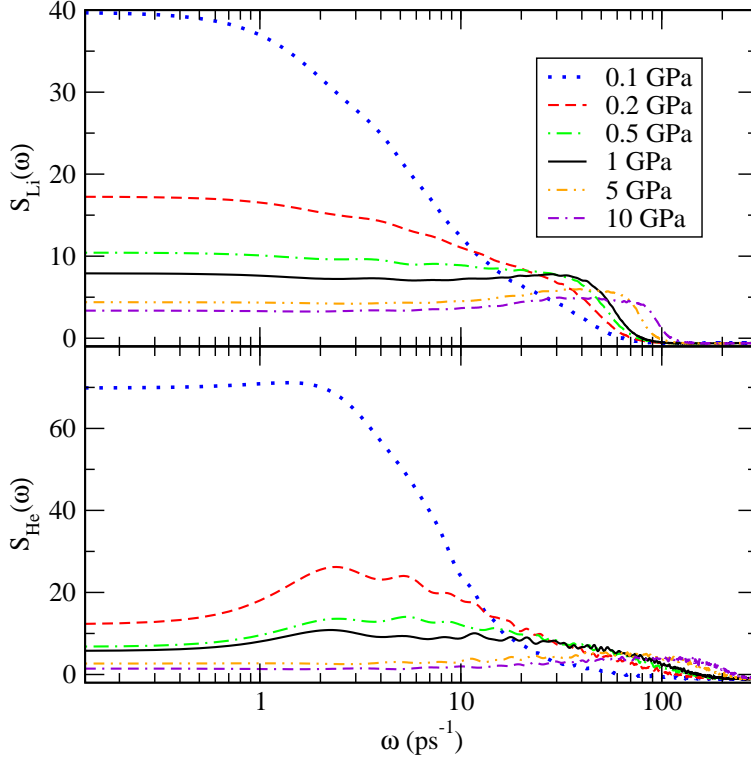


FIG. 10. Spectral densities of lithium (top) and helium (bottom) at 843 K as a function of pressure. Lines: 0.1 GPa (dotted blue); 0.2 GPa (dashed red); 0.5 GPa (dot-dashed green); 1 GPa (black); 5 GPa (dot-dot-dashed orange); 10 GPa (dash-dash-dotted violet).

In our simulations, helium atoms are miscible in the lithium bath at low pressures whereas, for pressures above some critical value, the mixture has the tendency to phase separate and split into pure lithium and pure helium phases (formation of helium droplets in the lithium background). This tendency is in overall contradiction with Henry's law, which has been observed experimentally to be met by liquid metals[46].

The simulations reported in this work are a first step towards the understanding of the phenomenon of helium nucleation in liquid lithium. Although our results do not agree with the behavior predicted by CNT, we have shown that the phenomenon of helium nucleation in liquid lithium at high temperatures and pressures can be captured by MD at its inception;

independently of the initial homogeneous disposition of atoms in the system, our simulation shows the formation of helium drops systematically if the same environmental conditions are met. Dynamical properties of the mixture such as diffusion coefficients of lithium and helium are very well reproduced, in overall good agreement with experimental data available. Better potential functions are to be tested in future studies which fit within the expected Henry's law behavior. Future studies would likely involve the calculation of surface tensions of the droplets and the analysis of the nucleation phenomenon on lithium-lead mixtures.

ACKNOWLEDGMENTS

We thank L.A.Sedano and A.Awad for fruitful discussions. J.M and L.B. acknowledge financial support from the Generalitat de Catalunya (project "FusionCAT", number J-02603). J.M. thanks the Spanish Ministry of Science, Innovation and Universities (project number PGC2018-099277-B-C21, funds MCIU/AEI/FEDER, UE). G.E.A. and F.M. acknowledge financial support from the Spanish MINECO (FIS2017-84114-C2-1-P), and from the Secretaria d'Universitats i Recerca del Departament d'Empresa i Coneixement de la Generalitat de Catalunya within the ERDF Operational Program of Catalunya (project QuantumCat, Ref. 001-P-001644).

-
- [1] M. Kordač and L. Košek, Helium bubble formation in pb-16li within the breeding blanket, *Fusion Engineering and Design* **124**, 700 (2017).
 - [2] G. Federici, L. Boccaccini, F. Cismondi, M. Gasparotto, Y. Poitevin, and I. Ricipito, An overview of the eu breeding blanket design strategy as an integral part of the demo design effort, *Fusion Engineering and Design* **141**, 30 (2019).
 - [3] M. Rubel, Fusion neutrons: tritium breeding and impact on wall materials and components of diagnostic systems, *Journal of Fusion Energy* **38**, 315 (2019).
 - [4] V. Coen, Lithium-lead eutectic as breeding material in fusion reactors, *Journal of nuclear materials* **133**, 46 (1985).
 - [5] E. M. De Les Valls, L. Sedano, L. Batet, I. Ricipito, A. Aiello, O. Gastaldi, and F. Gabriel, Lead–lithium eutectic material database for nuclear fusion technology, *Journal of nuclear*

TABLE I. Average internal energies (U), pressures (P) and temperatures (T) for the simulated setups. All MC simulations considered 10^8 sampling moves and all MD simulations were of total length 200 ps.

Method	U (K)	P (GPa)	T(K)
MC	71.1	0.104	843
	-187.0	0.122	843
	-430.3	0.146	843
	-553.3	0.178	843
	-700.0	0.208	843
	-1183.7	0.500	843
	-1398.6	1.005	843
	-1197.6	5.002	843
	-261.9	9.994	843
MD	150.8	0.105	842.3
	-214.2	0.128	842.1
	-380.4	0.152	842.1
	-507.6	0.177	842.1
	-720.8	0.202	841.9
	-1182.3	0.501	841.7
	-1405.2	0.999	841.6
	-1199.1	4.999	841.0
	-262.8	9.998	840.3

materials **376**, 353 (2008).

- [6] L. Sedano, Helium bubbles cavitation phenomena in pb-15.7 li and potential impact on tritium transport behaviour in hcll breeding channels. centro de investigaciones energeticas medioambientales y tecnologicas (ciemat, spain), (2007).
- [7] D. Ruzic, M. Szott, C. Sandoval, M. Christenson, P. Fifiis, S. Hammouti, K. Kalathiparambil, I. Shchelkanov, D. Andruczyk, R. Stubbers, et al., Flowing liquid lithium plasma-facing components—physics, technology and system analysis of the limit system, Nuclear Materials

TABLE II. Radii of helium drops at 843 K as a function of the pressure.

Pressure (GPa)	R_{He} (Å)
0.175	1.980
0.2	1.934
0.3	1.845
0.5	1.812
1	1.847
5	1.629
7	1.508
10	1.320

TABLE III. Diffusion coefficients of lithium and helium at 843 K as a function of the pressure.

Pressure (GPa)	D_{He} (Å ² /ps)	D_{Li} (Å ² /ps)
0.1	1.850	3.583
0.125	1.936	3.217
0.15	1.822	3.010
0.175	2.071	2.958
0.2	1.670	2.833
0.3	1.350	2.667
0.4	1.300	2.333
0.5	1.167	2.167
1	0.833	2.006
5	0.583	1.408
7	0.430	1.120
10	0.350	1.067

and Energy **12**, 1324 (2017).

- [8] S. Smolentsev, T. Rognlien, M. Tillack, L. Waganer, and C. Kessel, Integrated liquid metal flowing first wall and open-surface divertor for fusion nuclear science facility: Concept, design, and analysis, Fusion Science and Technology **75**, 939 (2019).

- [9] H. Nakamura, P. Agostini, K. Ara, S. Cevolani, T. Chida, M. Ciotti, S. Fukada, K. Furuya, P. Garin, A. Gessii, et al., Latest design of liquid lithium target in ifmif, Fusion Engineering and Design **83**, 1007 (2008).
- [10] J. W. Gibbs, On the equilibrium of heterogeneous substances, American Journal of Science **3**, 441 (1878).
- [11] J. W. Gibbs, Scientific Papers of J. Willard Gibbs, in Two Volumes, Vol. 1 (Longmans, Green, 1906).
- [12] L. Batet, J. Fradera, E. M. de les Valls, and L. Sedano, Numeric implementation of a nucleation, growth and transport model for helium bubbles in lead–lithium hell breeding blanket channels: Theory and code development, Fusion engineering and design **86**, 421 (2011).
- [13] F. Mazzanti, A. Polls, J. Boronat, and J. Casulleras, High-momentum response of liquid he3, Physical review letters **92**, 085301 (2004).
- [14] F. Mazzanti, G. Astrakharchik, J. Boronat, and J. Casulleras, Ground-state properties of a one-dimensional system of hard rods, Physical review letters **100**, 020401 (2008).
- [15] C. Pierleoni, M. A. Morales, G. Rillo, M. Holzmann, and D. M. Ceperley, Liquid–liquid phase transition in hydrogen by coupled electron–ion monte carlo simulations, Proceedings of the National Academy of Sciences **113**, 4953 (2016).
- [16] R. Bombin, J. Boronat, and F. Mazzanti, Dipolar bose supersolid stripes, Physical review letters **119**, 250402 (2017).
- [17] G. Mazzola, R. Helled, and S. Sorella, Phase diagram of hydrogen and a hydrogen-helium mixture at planetary conditions by quantum monte carlo simulations, Physical Review Letters **120**, 025701 (2018).
- [18] J. Sánchez-Baena, J. Boronat, and F. Mazzanti, Supersolid stripes enhanced by correlations in a raman spin-orbit-coupled system, Physical Review A **101**, 043602 (2020).
- [19] J. Martí and M. Gordillo, Microscopic dynamics of confined supercritical water, Chemical physics letters **354**, 227 (2002).
- [20] G. Nagy, M. Gordillo, E. Guàrdia, and J. Martí, Liquid water confined in carbon nanochannels at high temperatures, The Journal of Physical Chemistry B **111**, 12524 (2007).
- [21] P. Videla, J. Sala, J. Martí, E. Guàrdia, and D. Laria, Aqueous electrolytes confined within functionalized silica nanopores, The Journal of chemical physics **135**, 104503 (2011).
- [22] J. Sala, E. Guardia, and J. Martí, Specific ion effects in aqueous eletrolyte solutions confined

- within graphene sheets at the nanometric scale, *Physical Chemistry Chemical Physics* **14**, 10799 (2012).
- [23] C. Calero, J. Martí, and E. Guàrdia, 1h nuclear spin relaxation of liquid water from molecular dynamics simulations, *The Journal of Physical Chemistry B* **119**, 1966 (2015).
 - [24] M. Gordillo and J. Martí, Hydrogen bond structure of liquid water confined in nanotubes, *Chemical Physics Letters* **329**, 341 (2000).
 - [25] H. A. Zambrano, J. H. Walther, P. Koumoutsakos, and I. F. Sbalzarini, Thermophoretic motion of water nanodroplets confined inside carbon nanotubes, *Nano letters* **9**, 66 (2009).
 - [26] J. Rodriguez, M. D. Elola, J. Martí, and D. Laria, Surface behavior of aprotic mixtures: dimethyl sulfoxide/acetonitrile, *The Journal of Physical Chemistry C* **121**, 14618 (2017).
 - [27] M. Karplus and G. Petsko, Molecular dynamics simulations in biology, *Nature* **347**, 631 (1990).
 - [28] M. Karplus and J. McCammon, Molecular dynamics simulations of biomolecules, *Nature structural biology* **9**, 646 (2002).
 - [29] J. Martí and F. Csajka, Transition path sampling study of flip-flop transitions in model lipid bilayer membranes, *Phys. Rev. E* **69**, 061918 (2004).
 - [30] J. Yang, C. Calero, and J. Martí, Diffusion and spectroscopy of water and lipids in fully hydrated dimyristoylphosphatidylcholine bilayer membranes, *The Journal of chemical physics* **140**, 03B606.1 (2014).
 - [31] K. A. Yakimovich and A. G. Mozgovoï, Experimental investigation of the density and surface tension of molten lithium at temperatures up to 1300 k, *High Temperature* **38**, 657 (2000).
 - [32] M. Canales, J. Padró, L. González, and A. Giró, Molecular dynamics simulation of liquid lithium, *Journal of Physics: Condensed Matter* **5**, 3095 (1993).
 - [33] M. Canales, L. González, and J. Padró, Computer simulation study of liquid lithium at 470 and 843 k, *Physical Review E* **50**, 3656 (1994).
 - [34] R. A. Aziz, F. R. McCourt, and C. C. Wong, A new determination of the ground state interatomic potential for he2, *Molecular Physics* **61**, 1487 (1987).
 - [35] X. Zhou, N. Bartelt, and R. Sills, Enabling simulations of helium bubble nucleation and growth: A strategy for interatomic potentials, *Physical Review B* **103**, 014108 (2021).
 - [36] N. Juslin and B. Wirth, Interatomic potentials for simulation of he bubble formation in w, *Journal of Nuclear Materials* **432**, 61 (2013).
 - [37] D. Frenkel and B. Smit, Understanding molecular simulation: from algorithms to applications,

- Vol. 1 (Elsevier, 2001).
- [38] L. Wang, Discovering phase transitions with unsupervised learning, *Physical Review B* **94**, 195105 (2016).
 - [39] C. Jayaram, R. Ravi, and R. Chhabra, Calculation of self-diffusion coefficients in liquid metals based on hard sphere diameters estimated from viscosity data, *Chemical physics letters* **341**, 179 (2001).
 - [40] M. Nieto, D. Ruzic, J. P. Allain, M. Coventry, and E. Vargas-Lopez, Helium retention and diffusivity in flowing liquid lithium, *Journal of nuclear materials* **313**, 646 (2003).
 - [41] D. A. McQuarrie, Statistical Mechanics (University Science Books, 2000).
 - [42] J. Martí, J. Padró, and E. Guàrdia, Computer simulation of molecular motions in liquids: Infrared spectra of water and heavy water, *Molecular Simulation* **11**, 321 (1993).
 - [43] J. Martí, E. Guardia, and J. Padró, Dielectric properties and infrared spectra of liquid water: Influence of the dynamic cross correlations, *J. Chem. Phys.* **101**, 10883 (1994).
 - [44] M. Praprotnik and D. Janežič, Molecular dynamics integration and molecular vibrational theory. iii. the infrared spectrum of water, *J. Chem. Phys.* **122**, 174103 (2005).
 - [45] J. Padró and J. Martí, Response to “comment on ‘an interpretation of the low-frequency spectrum of liquid water’” [*j. chem. phys.* 118, 452 (2003)], *The Journal of Chemical Physics* **120**, 1659 (2004).
 - [46] H. Slotnick, The solubility of helium in lithium and potassium, Vol. 380 (Pratt & Whitney Aircraft Division, United Aircraft Corporation, CANEL Operations, 1965).